Predictive Control of an Axial Flux Permanent Magnet Synchronous Machine

Essay awarded in 2017 by the Koninklijke Belgische Vereniging der Elektrotechnici

Lynn Verkroost[1,2]
[1]Dpt. Electrical Energy, Metals, Mechanical Constructions & Systems,
Ghent University, B-9000 Ghent, Belgium
Email: Lynn.Verkroost@UGent.be
[2]EEDT, Flanders Make

Joachim Druant[1,2], Hendrik Vansompel[1,2],
Frederik De Belie[1,2] and Peter Sergeant[1,2]
[1]Dpt. Electrical Energy, Metals, Mechanical Constructions & Systems,
Ghent University, B-9000 Ghent, Belgium
[2]EEDT, Flanders Make

***Abstract*—This paper examines the (dis)advantages of predictive control for the torque regulation of an axial flux permanent magnet synchronous machine fed by a two-level voltage source inverter. Three different types of predictive controllers are studied: finite-set model based predictive control, deadbeat control and finite-set model based predictive control with duty cycle calculation. A standard PI controller is added to provide a benchmark. The real-life performance of the control algorithms is tested on a 4 kW laboratory drive setup. It is concluded that the PI controller shows superior steady-state behavior, whereas the predictive controllers excel when it comes to dynamic performance.**

I. Introduction

The recent focus on ecodesign led to the development of new electrical machine topologies, such as the axial flux permanent magnet synchronous machine (AFPMSM). Its high power density and efficiency make this topology very suitable for integration in electrical drive trains for sustainable energy conversion, and industrial and transport applications [1]. Many of these applications require that the torque of the AFPMSM is regulated. Due to the emergence of fast control hardware platforms like field programmable gate arrays (FPGAs), predictive control became a full-fledged alternative for the commonly used PI controllers for electric drives with time constants in the millisecond range [2]. After all, predictive controllers make use of a mathematical system model to predict the system behavior, and this model needs to be evaluated at least two times per update period of the controller.

In this paper, the focus will be on two prominent families in the large collection of predictive controllers: finite-set model based predictive control (FS-MBPC) and deadbeat (DB) control. In addition, a third controller combining the features of these two families will be studied as well: FS-MBPC with duty cycle calculation. However, the non-predictive PI controller is still one of the most frequently used controllers in industry. The purpose of this paper is therefore to compare the predictive controllers not only with each other, but also with this standard PI controller. To achieve this goal, the four controllers are implemented on a 4 kW prototype of an AFPMSM fed by a two-level voltage source inverter (2L-VSI). Some key performance indicators (KPIs) are defined to enable a quantitative comparison of the performance of the different controllers.

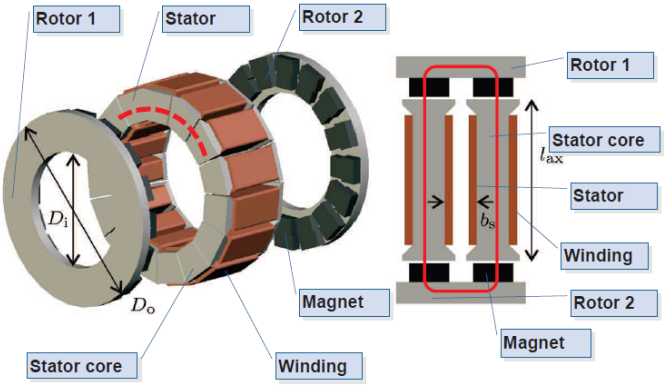

Fig. 1: The AFPMSM with YASA topology, consisting of one stator with multiple stator cores, and two rotors with permanent magnets

II. System Description

A. Axial Flux Permanent Magnet Synchronous Machine

The AFPMSM used in this paper has a yokeless and segmented armature (YASA) topology and is shown in Fig. 1. The machine consists of one stator, and two rotors with surface-mounted permanent magnets (PMs). The flux crosses the air gap in the axial direction.

B. Two-Level Voltage Source Inverter

The AFPMSM is fed by a 2L-VSI, shown in Fig. 2a. The six switches S_x, $\overline{S}_x$ ($x \in \{a, b, c\}$) connect the load to either the positive or the negative DC-bus voltage. This results in eight possible switch states $S = [S_a; S_b; S_c]$, corresponding to the voltage vectors in Fig. 2b. $\underline{V}_0$ and $\underline{V}_7$ are called the null vectors, the other six vectors are the active voltage vectors.

III. Control Algorithms

In Fig. 3 is illustrated that the goal of the controllers is to determine the switch state S of the 2L-VSI, based

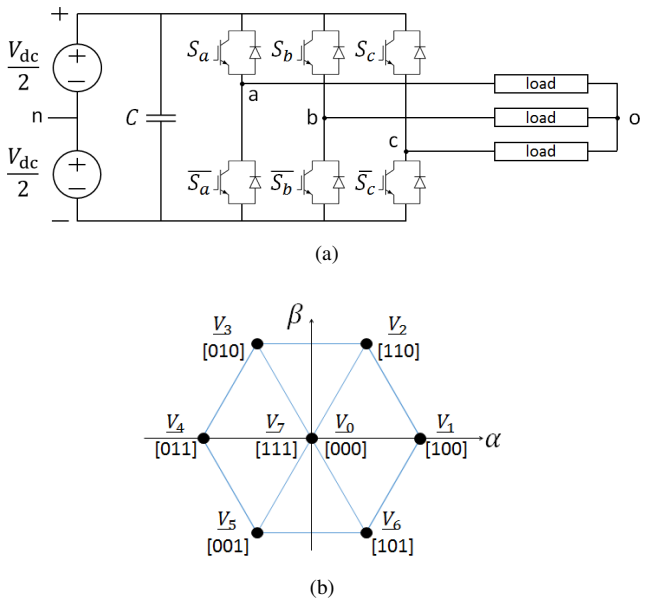

Fig. 2: The 2L-VSI: (a) topology, (b) the eight possible voltage vectors

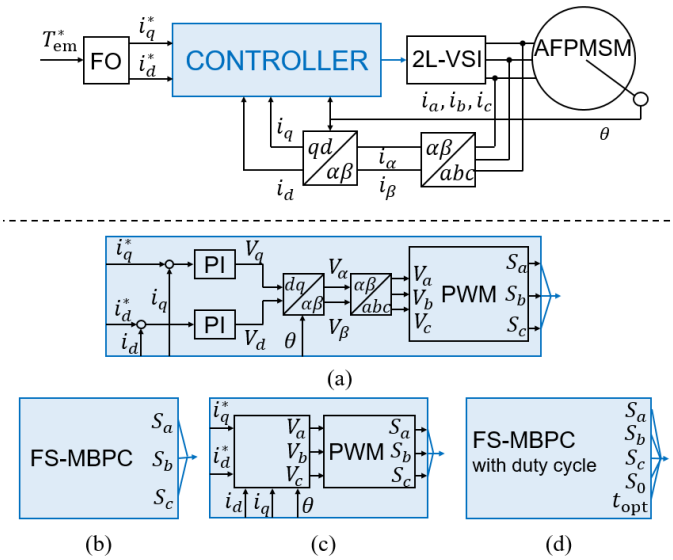

Fig. 3: General control scheme, with the four examined controllers: (a) PI control, (b) FS-MBPC, (c) DB control, (d) FS-MBPC with duty cycle calculation

on the required torque T^*_{em}, the measured rotor position θ, and the measured stator currents i_a, i_b, i_c. The so-called field orientation (FO) principle is used for this purpose. This principle requires that the stator current components i_a, i_b, i_c are transformed to the synchronous dq-reference frame, which is rotating synchronously with the rotor. The current component i_q is proportional to the torque T_{em} in this way. To avoid unnecessary copper losses, the current component i_d is kept equal to zero throughout this text. Hence, the field orientation principle transforms the reference value for the torque T^*_{em} into reference values for the current components i^*_q and i^*_d.

A. PI Control

Field orientation is frequently implemented by means of two standard PI controllers. The control scheme in Fig. 3a shows that the PI controllers determine reference values for the voltage components v_q and v_d, based on the error in the current components i_q and i_d. These voltage components are first transformed back to the abc-reference frame, after which this abc-reference voltage is translated into a switching sequence for the 2L-VSI by means of pulse width modulation (PWM). For the application discussed in this paper, root locus techniques were applied to a linearized model to determine the PI parameters $K_p = 4.13$ V/A and $K_i = 3206.4$ V/As.

B. Finite-Set Model Based Predictive Control

FS-MBPC is often employed for the control of electrical machines fed by an inverter [2]–[6]. This control strategy uses a system model to forecast the future machine state (torque, flux, and current) for each of the eight possible switch states S of the 2L-VSI. For each switch state, a cost function is evaluated. Eventually, the switch state with the lowest cost is selected, and applied to the system. The control scheme

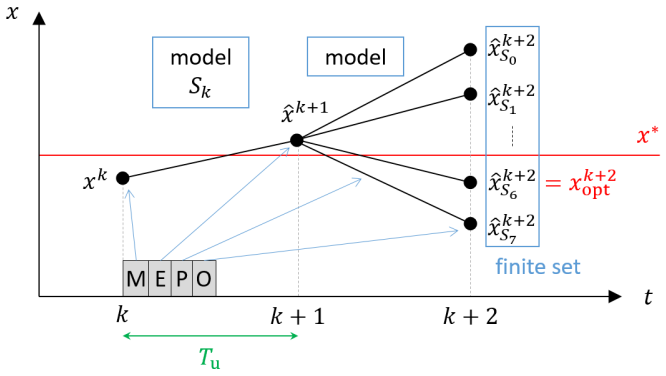

Fig. 4: Working principle of FS-MBPC, illustrating the four basic steps: measurement (M), estimation (E), prediction (P), and optimization (O)

is shown in Fig. 3b, and the working principle is presented schematically in Fig. 4. Four basic steps can be distinguished during one update period T_{u} of the controller: measurement, estimation, prediction and optimization. The latter three will be elucidated in the next sections.

1) Estimation: At the discrete time instant k, the optimal switch state S_k (determined during the previous update period $k-1 \rightarrow k$) is applied, and the stator current and rotor position are measured. With this information, the current components $\hat{i}_q^{k+1}$ and $\hat{i}_d^{k+1}$ at time instant $k+1$ are estimated by means of the system model. This estimation step is necessary, since i_q^{k+1} and i_d^{k+1} need to be known for the calculation of the optimal input S_{k+1} at instant $k+1$. Directly measuring the current at instant $k+1$ is not an option, since this would require that the controller is able to determine S_{k+1} in an infinitesimally small period of time.

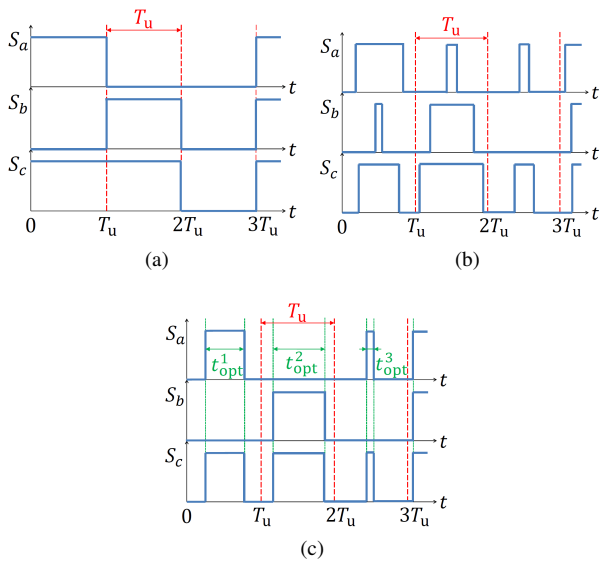

Fig. 5: Difference in switching between (a) FS-MBPC, (b) PI and DB control, (c) FS-MBPC with duty cycle calculation

2) Prediction: For each of the eight possible switch states S_{k+1}, the variables i_q^{k+2} and i_d^{k+2} at time instant $k+2$ are calculated by means of the system model, starting from the estimates $\hat{i}_q^{k+1}$ and $\hat{i}_d^{k+1}$.

3) Optimization: Based on the evaluation of a cost function, the most appropriate switch state S_{k+1} is selected, bringing the current components closest to their desired values $i_q^{k,*}$ and $i_d^{k,*}$. Since there is only a finite-set of switch states, no complex or time-consuming minimization algorithm is needed: calculating the cost for every single switch state and picking the one leading to the smallest cost suffices. This optimal switch state S_{k+1} is then applied to the system during the entire following update period $k+1 \rightarrow k+2$, after which the algorithm is restarted.

An example of a switching sequence is provided in Fig. 5a. An important drawback of FS-MBPC is that the switching frequency may vary - as the switch state will not change at every update instant - making it harder to design a proper electromagnetic interference filter. A major advantage of FS-MBPC, on the other hand, is the fact that secondary control goals, like for instance minimization of the switching losses, can be easily expressed by adding extra terms to the cost function.

C. Deadbeat Control

Contrary to FS-MBPC, DB control makes use of the system model to calculate which input voltage is required to bring the current components i_q and i_d to their reference values i_q^* and i_d^* in one time step [3], [4], [7]. This reference value for the voltage is applied to the machine by means of PWM, just as for the PI controller. The control scheme is shown in Fig. 3c; the working principle is presented in Fig. 6. Three basic steps can be distinguished: measurement, estimation, and deadbeat. The latter two are discussed extensively in the following sections.

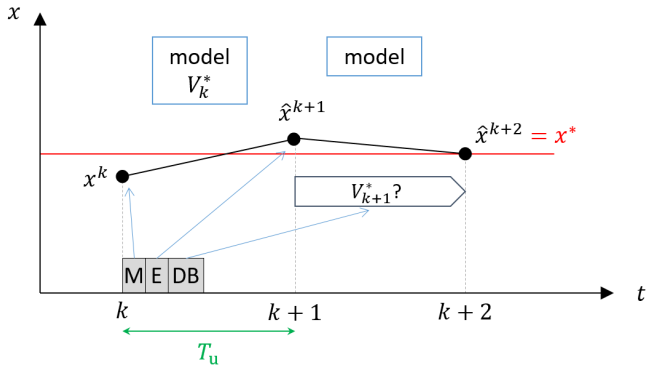

Fig. 6: Working principle of DB control, illustrating the three basic steps: measurement (M), estimation (E), and deadbeat (DB)

1) Estimation: The reference voltage V_k^* - determined during the previous period $k-1 \rightarrow k$ and applied to the machine by means of PWM during the period $k \rightarrow k+1$ - together with the measured current components and rotor position are used to estimate $\hat{i}_q^{k+1}$ and $\hat{i}_d^{k+1}$ by means of the system model.

2) Deadbeat: To determine the reference voltage V_{k+1}^*, the system model is evaluated under the assumption that at time instant $k+2$ the current components equal their reference values: $\hat{i}_q^{k+2} = i_q^{k,*}$ and $\hat{i}_d^{k+2} = i_d^{k,*}$. Contrary to FS-MBPC, which limits the voltage to the discrete set of eight voltage vectors corresponding to the eight switch states of the 2L-VSI, the DB controller allows to apply every real voltage value within the limits of the DC-bus. The DB controller is followed by a PWM algorithm, which determines the switching sequence for the 2L-VSI that causes the average applied voltage during the period $k \rightarrow k+1$ to equal its reference value. This results in the same switching behavior as for the PI controller, which is shown in Fig. 5b.

Apart from the additional freedom in the applicable voltage, another advantage of DB control is that it requires less computational effort than FS-MBPC: the system model needs to be evaluated only once in the deadbeat step, whereas FS-MBPC requires a system evaluation for each possible switch state in the prediction step. Even when the algorithms are implemented on an FPGA - which enables the use of a pipeline for the system evalution for each switch state - the FS-MBPC algorithm still requires 1.11 μs, whereas the DB algorithm only needs 0.97 μs. However, a disadvantage of the DB algorithm is that it does not make use of a cost function. Hence, secondary control goals are more difficult to take into account. Therefore, a controller combining the advantages of both FS-MBPC and DB control will be presented in the next section.

D. FS-MBPC with Duty Cycle Calculation

FS-MBPC with duty cycle calculation combines the features of standard FS-MBPC and DB control. The working principle is the same as for standard FS-MBPC, with the only difference

that the DB principle is used to determine an appropriate duty cycle for each of the six active voltage vectors of the 2L-VSI [3], [9]–[11]. The resulting switching behavior is presented in Fig. 5c; the control scheme is given in Fig. 3d.

1) Estimation: The stator current and rotor position (measured at instant k) are used together with the optimal combination of switch state and duty cycle $[S_k, t_{\text{opt}}^k]$ (determined during the previous update period $k-1 \rightarrow k$) to estimate $\hat{i}_q^{k+1}$ and $\hat{i}_d^{k+1}$ by means of the system model.

2) Prediction: Contrary to standard FS-MBPC, the active voltage vectors are now applied to the system for only a fraction of the update period. For the remainder of the update period, a null vector is applied. In order to determine a suitable duty cycle for each active voltage vector, the evolution of i_q and i_d under the active voltage vectors and the null vectors is computed. With this information is calculated for how long each active voltage vector needs to be applied in order to approach the reference i_q^* as close as possible.

3) Optimization: The optimal combination of active voltage vector and duty cycle is selected by means of a cost function. The usage of a cost function facilitates the expression of secondary control goals in comparison to DB control. The introduction of the duty cycle provides the possibility to vary the amplitude of the six active voltage vectors of the 2L-VSI, which is an additional degree of freedom compared to standard FS-MBPC. A disadvantage, however, is the fact that the calculation of the duty cycle increases the computational effort: evaluation of this algorithm takes 1.23 μs when implemented on an FPGA, whereas standard FS-MBPC requires only 1.11 μs.

IV. Comparison of the Controllers

To compare the performance of the four controllers, they are experimentally tested on the 4 kW test setup schematically presented in Fig. 7. A DC-bus voltage V_{dc} of 250 V is applied, and the mechanical speed N of the AFPMSM is maintained at 1000 rpm by an induction machine (IM) that is connected to the AFPMSM as load. The chosen update frequency f_{u} amounts to 10 kHz. The specifications of the AFPMSM - designed according to the principles proposed in [1] - are given in Table I. The control algorithms are implemented on a Xilinx©Kintex©-7 XC7K325T FPGA embedded in a dSPACE MicroLabBox. The FPGA is programmed using the Xilinx System Generator blockset in a MATLAB©&Simulink© environment.

The experimental results for the four types of controllers are presented in Fig. 8. All examined control strategies are able to track the reference value for the current component i_q, which is - according to the field orientation principle - proportional to the torque.

A. Control Quality

The difference in current ripple - and thus torque ripple - strikes immediately in Fig. 8. Apart from the fact that this ripple causes extra vibrations and noise, it also results in additional stator core losses and eddy current losses in the

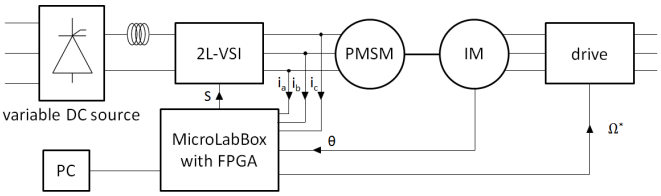

Fig. 7: Experimental test setup

TABLE I: Machine parameters

Parameter	Symbol	Value
Number of pole pairs	N_p	8
Rated power (kW)	P_{n}	4
Rated speed (rpm)	N_{n}	2500
Rated torque (Nm)	T_{n}	15
Rated voltage (V)	V_{n}	152
Stator inductance (mH)	$L_q = L_d$	2.54
Stator resistance (mΩ)	R_{s}	325
Mechanical inertia (kg·m^2)	J	0.0024
Equivalent PM current (A)	i_{mag}	-43.2

permanent magnets. To quantify the ripple, the mean absolute deviation (MAD) of the i_q measurements from their mean value is computed. The results shown in Fig. 9a reveal the superior performance of the PI and DB controller. FS-MBPC, on the other hand, displays the largest current ripple. Although the addition of the duty cycle calculation to standard FS-MBPC reduces the MAD, Fig. 8 shows that the maximal amplitude of the current ripple is still as high as for the standard algorithm under the considered test conditions. Moreover, the total harmonic distortion (THD) of the stator current, presented in Fig. 9b, is slightly increased by adding the duty cycle calculation. The stator current waveform of phase a and its harmonic spectrum - given in respectively Fig. 10 and 11 - confirm that the current has the largest distortion for FS-MBPC

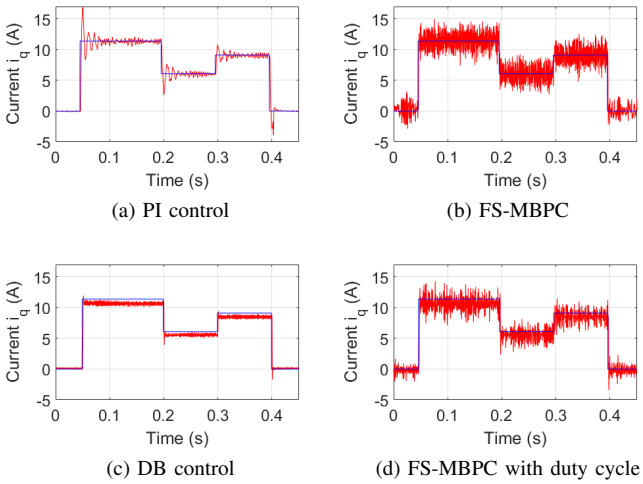

(a) PI control (b) FS-MBPC

(c) DB control (d) FS-MBPC with duty cycle

Fig. 8: Experimental results for i_q - which is proportional to the torque T_{em} - for $V_{\text{dc}} = 250$ V and $N = 1000$ rpm (blue: reference, red: measurement)

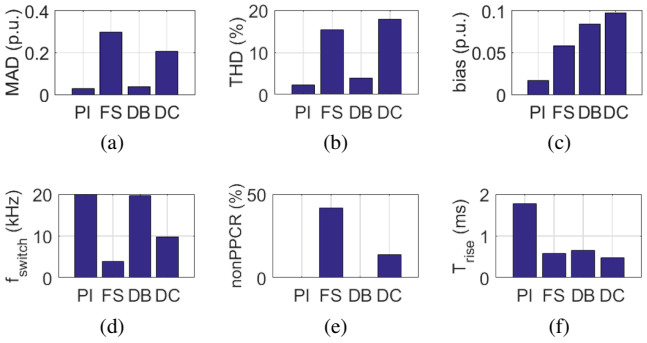

Fig. 9: Experimental key performance indicators for PI control (PI), FS-MBPC (FS), DB control (DB) and FS-MBPC with duty cycle calculation (DC)

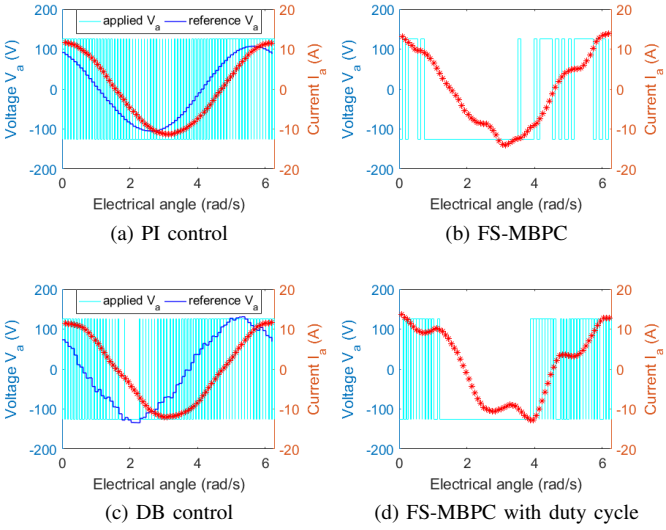

Fig. 10: Voltage and current waveforms of phase a for the four controllers ($V_{\mathrm{dc}} = 250$ V and $N = 1000$ rpm)

with duty cycle calculation, and the smallest distortion for PI control.

Since the main goal of the controllers is to track the reference value for i_q precisely, also the systematic deviation of the measured stator current from its reference value is of importance. This so-called bias is presented in Fig. 9c. The experiments show that only the predictive controllers - and especially the controllers making use of the DB principle - suffer from this disadvantage.

B. Voltage Quality

As FS-MBPC does not allow the switch state of the 2L-VSI to be changed during an update period of the controller - whereas this is possible for the other three controllers - its switching frequency and the related switching losses are lower than for the other examined controllers, as is illustrated both in Fig. 9d and in the voltage waveforms of phase a given in Fig. 10. However, the switch state changes that do take place

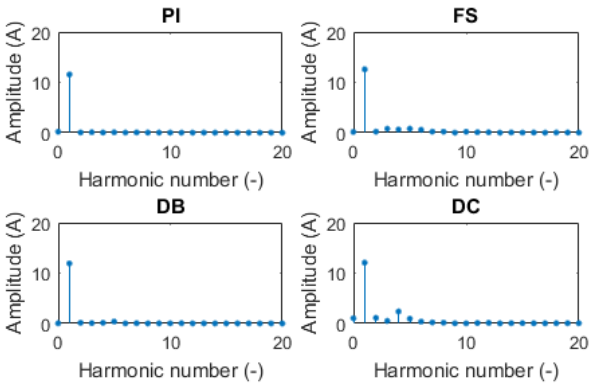

Fig. 11: Current harmonics of phase a ($V_{\mathrm{dc}} = 250$ V and $N = 1000$ rpm)

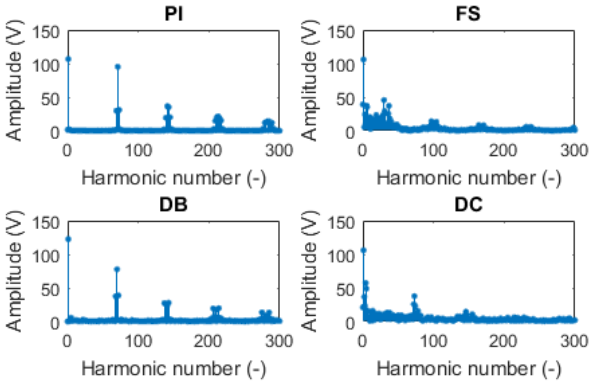

Fig. 12: Voltage harmonics of phase a ($V_{\mathrm{dc}} = 250$ V and $N = 1000$ rpm)

violate the pulse polarity consistency rule (PPCR) in 40% of the cases. For a 2L-VSI, the PPCR implies that switching can only happen between two neighboring voltage vectors, in order not to burden the machine isolation. Fig. 9e indicates that the increase in switching frequency when duty cycle calculation is added to FS-MBPC causes the PPCR to be fulfilled more often. For DB and PI control, almost no violations of the PPCR occur anymore. The voltage spectra presented in Fig. 12 show that the voltage applied by FS-MBPC still contains harmonics that are too low to be adequately filtered out by the inductive character of the AFPMSM. The PWM algorithm used by the DB and PI controller, on the other hand, shifts the harmonics to much higher orders.

C. Dynamic Behavior

Regarding the dynamic behavior, only the DB and PI controller show distinct overshoot peaks in the step response of i_q. Furthermore, in Fig. 9f can be seen that the rise time required to reach the reference value of i_q is significantly higher for the PI controller than for the predictive controllers.

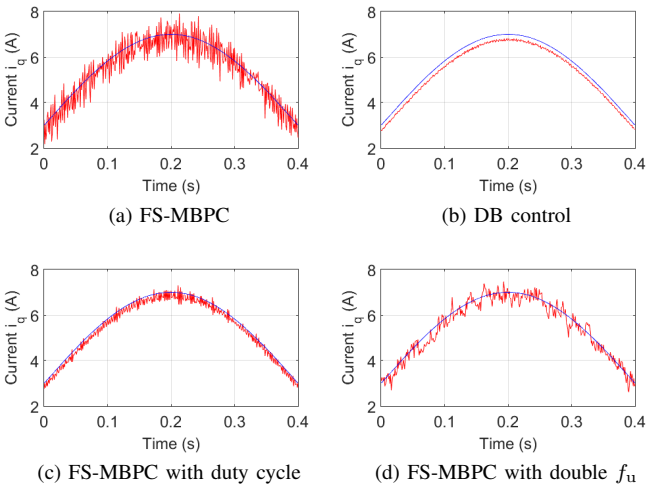

(a) FS-MBPC (b) DB control

(c) FS-MBPC with duty cycle (d) FS-MBPC with double f_{u}

Fig. 13: Experimental results for i_q - which is proportional to the torque T_{em} - for $V_{\mathrm{dc}} = 100$ V and $N = 300$ rpm (blue: reference, red: measurement)

D. Influence of the Working Conditions

The foregoing comparison is based on the experimental results of Fig. 8, measured at a DC-bus voltage $V_{\mathrm{dc}} = 250$ V and mechanical speed $N = 1000$ rpm. Under these working conditions, the control quality of FS-MBPC with duty cycle calculation is slightly disappointing: it was expected that the control quality would improve due to the additional degree of freedom in the applicable voltage, but the addition of the duty cycle actually deteriorated the performance of the standard FS-MBPC. However, when working under $V_{\mathrm{dc}} = 100$ V and $N = 300$ rpm, addition of the duty cycle calculation does reduce the current ripple - and thus the torque ripple - compared to standard FS-MBPC, as can be seen by comparing Fig. 13a and 13c. This makes FS-MBPC with duty cycle calculation an excellent choice for applications which do not allow the high torque ripple of standard FS-MBPC, but should have less switching losses than DB or PI control, or should have the ability to express secondary control goals easily. Comparison of Fig. 13a and 13d shows that doubling the update frequency f_{u} of standard FS-MBPC effectively reduces the torque ripple as well. However, this option doubles the computational effort. In general can be stated that the torque ripple reduces for reduced DC-bus voltage and reduced speed for all the controllers: the DB controller, for instance, shows less ripple in Fig. 13b than in Fig. 8c. The main reason for this phenomenom is the fact that a lower immediate voltage is applied to the phase coils when the switches of the 2L-VSI connect the phases to a lower DC-bus voltage, resulting in a decreased current derivative. The effect of the speed can be explained in a similar way, as the back-EMF decreases with the speed.

V. Conclusion

The performance of three different predictive current controllers and a PI controller have been compared on a test setup of a 4 kW AFPMSM fed by a 2L-VSI. For this purpose some KPIs were introduced. It was concluded that the PI controller outweighs the predictive controllers concerning steady-state control quality: only the DB controller can compete with its low torque ripple. The predictive controllers, on the other hand, excel in dynamic performance.

References

[1] H. Vansompel, P. Sergeant, L. Dupré, and A. Van Den Bossche, "Axial-flux PM machines with variable air gap," *IEEE Trans. Ind. Electron.*, vol. 61, no. 2, pp. 730–737, 2014.

[2] T. J. Vyncke, S. Thielemans, and J. A. Melkebeek, " Finite-Set Model-Based Predictive Control for Flying-Capacitor Converters: Cost Function Design and Efficient FPGA Implementation," *IEEE Trans. Ind. Informatics*, vol. 9, no. 2, pp. 1113–1121, 2013.

[3] F. Morel, X. Lin-Shi, J.-M. Rétif, B. Allard, and C. Buttay, "A comparative study of predictive current control schemes for a permanent-magnet synchronous machine drive," *IEEE Trans. Ind. Electron.*, vol. 56, no. 7, pp. 2715–2728, 2009.

[4] W. Xie et al., "Finite-control-set model predictive torque control with a deadbeat solution for PMSM drives," *IEEE Trans. Ind. Electron.*, vol. 62, no. 9, pp. 5402–5410, 2015.

[5] T. Vyncke, S. Thielemans, M. Jacxsens, and J. Melkebeek, "Analysis of some design choices in model based predictive control of flying-capacitor inverters," *COMPEL - The Int. J. Comput. Math. Electr. Electron. Eng.*, vol. 31, no. 2, pp. 619–635, 2012.

[6] S. Kouro, P. Cortés, R. Vargas, U. Ammann, and J. Rodriguez, "Model predictive control - A simple and powerful method to control power converters," *IEEE Trans. Ind. Electron.*, vol. 56, no. 6, pp. 1826–1838, 2009.

[7] H. Zhu, X. Xiao, and Y. Li, "Torque ripple reduction of the torque predictive control scheme for permanent-magnet synchronous motors," *IEEE Trans. Ind. Electron.*, vol. 59, no. 2, pp. 871–877, 2012.

[8] B. H. Kenny and R. D. Lorenz, "Stator and rotor flux based deadbeat direct torque control of induction machines," *IEEE Trans. Ind. Appl.*, vol. 39, no. 4, pp. 1093–1101, 2003.

[9] Y. Zhang and H. Yang, "Model predictive torque control of induction motor drives with optimal duty cycle control," *IEEE Trans. Power Electron.*, vol. 29, no. 12, pp. 6593–6603, 2014.

[10] Y. Zhang, H. Yang, and B. Xia, "Model predictive torque control of induction motor drives with reduced torque ripple," *IET Electr. Power Appl.*, vol. 9, no. 9, pp. 595–604, 2015.

[11] M. Nemec, D. Nedeljkovic, and V. Ambrozic, "Predictive Torque Control of Induction Machines Using Immediate Flux Control," *IEEE Trans. Ind. Electron.*, vol. 54, no. 4, pp. 2009–2017, 2007.